

Article

Not peer-reviewed version

CAMPBOR SULFONIMINE COMPOUNDS: BOTTOM-UP DESIGN OF MOF'S FROM ORGANIC FRAMEWORKS BASED ON X-RAYS AND DFT-D3

[Adelino M. Galvão](#)*, [Joana P. Costa](#), [M. Fernanda N. N. Carvalho](#)

Posted Date: 26 September 2023

doi: 10.20944/preprints202309.1759.v1

Keywords: DFT-D3; self-assembly; camphor sulfonimine; X-ray diffraction; redox properties; complexes; non-bonding interactions



Preprints.org is a free multidiscipline platform providing preprint service that is dedicated to making early versions of research outputs permanently available and citable. Preprints posted at Preprints.org appear in Web of Science, Crossref, Google Scholar, Scilit, Europe PMC.

Copyright: This is an open access article distributed under the Creative Commons Attribution License which permits unrestricted use, distribution, and reproduction in any medium, provided the original work is properly cited.

Article

Camphor Sulfonylimine Compounds: Bottom-Up Design of MOF's from Organic Frameworks Based on X-rayS and DFT-D3

Joana P. Costa ^a, M. Fernanda N.N. Carvalho ^a and Adelino M. Galvão ^{b,*}

^a Centro de Química Estrutural, Institute of Molecular Sciences and Departamento de Engenharia Química, Instituto Superior Técnico, Universidade de Lisboa, Avenida António José de Almeida, n.º 12, 1000-043 Lisboa, Portugal.

^b Centro de Química Estrutural, Institute of Molecular Sciences and Departamento de Engenharia Química, Instituto Superior Técnico, Campus Taguspark, Universidade de Lisboa, Av. Prof. Doutor Cavaco Silva 2744-016 Porto Salvo, Portugal,

* Correspondence: E-mail: adelino@tecnico.ulisboa.pt.

Abstract: DFT-D3 calculations based on structural X-ray diffraction data obtained for 3-oxo-camphorsulfonyl imine (**1**), camphorsulfonyl chloride (**2**) and seven camphor sulfonylimines ($O_2SNC_{10}H_{13}NR$, **L**¹-**L**⁷) from which **L**² ($R=4-OHC_6H_4$), **L**⁴ ($R=4-ClC_6H_4$) and **L**⁶ ($R=3,5-(CH_3)_2C_6H_3$) are new, provide information into the *intra* and *inter* molecular interactions with concomitant elucidation of the supramolecular arrangement of the compounds. The DFT-D3 calculations performed in small clusters of 2 or 3 molecular units reproduce the interactions observed by X-ray analyses showing that as a general trend the structural arrangement of the molecules is driven by electronic rather than by packing parameters. In all compounds the self-assembly of 3D structures involves the sulfonyl imine group ($-NSO_2$) either to establish hydrogen bonds, through the oxygen atoms or non-classic oxygen-aliphatic hydrogen or non-bonding interactions (NBI) which also involve the sulfonyl oxygens. Interestingly, the camphor sulfonylimine compounds (**L**², **L**³) having protic groups ($R=C_6H_4X$: $X=OH$, **L**² or $X=NH_2$, **L**³) at the aromatic imine substituents ($=NR$) present an extra π - π stacking which is absent in the other compounds aromatic derivatives. The X-ray analysis shows that all the reported camphor sulfonylimine compounds display the *E* configuration with respect to the imine substituent (*R*). The study of the redox behavior of the compounds by cyclic voltammetry allows an insight into the solution properties of the compounds and the rationalization of the molecular interactions that stand in the solid and solution states. Camphor sulfonylimine compounds (**L**) display appropriate binding atoms to coordinate transition metals. The herein results show that monodentate coordination through the nitrogen atom of the sulfonylimine 5-membered ring to the $\{Ag(NO_3)\}$ metal center is favored. When this imine nitrogen atom is not itself involved in the Organic Framework DFT-D3 calculations shows that the complexation does not affect the non-covalent interactions that are reproduced in the MOF structure.

Keywords: DFT-D3; self-assembly; camphor sulfonylimine; X-ray diffraction; redox properties; complexes; non-bonding interactions

1. Introduction

The molecular structure of coordination compounds is formed by organic and inorganic moieties that combine to form new metal-ligand interactions. The formation of the new compounds can involve a major change into the pre-existing structural arrangement of the ligand or the metal precursors or, be shaped through binding of one of them, into the pre-organized structures of the other without a major reorganization.

In the case of complexes based on neutral ligands, covalent dative bonds are established involving the ligand heteroatoms lone pair (e.g. N, O, S) without change in the metal oxidation state

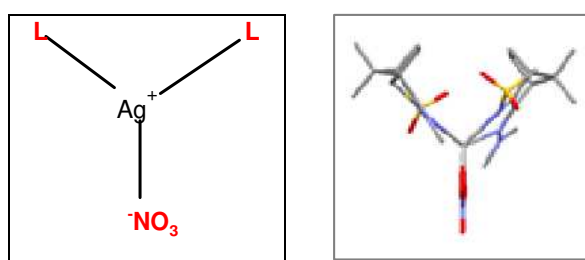
or modification of the ligand composition. That is the case of camphor sulfonimines ($\text{RNC}_{10}\text{H}_{13}\text{NSO}_2$) that typically bind the metal through the nitrogen lone pair ($=\text{NSO}_2$) forming dative bonds that in some cases are reinforced by Van der Waals interactions (non-bonding interactions, NBI) involving the imine nitrogen atom ($=\text{NR}$) [1–3].

Pre-existing intermolecular NBI in the organic or inorganic scaffolds can be maintained or be broken within the formation of the coordination compound. If the NBI remain, the coordination compound eventually acquires a polymeric character. NBI play a significant role in the structural, reactivity and selectivity of the coordination compounds [4,5] and are referred as being the primary transport mechanism by which thermal conductivity is increased in cross-linked polymers [6].

In some cases a structure/reactivity relationship can be established in complexes [7,8] allowing properties prediction based on the structure, *e.g.* biological and/or catalytic properties of camphor sulfonimine coordination compounds. [3,9] Unfortunately, the structural analysis of coordination compounds based on X-ray diffraction is sometimes impossible due to no suitable crystal are obtained. However, if X-ray data on the organic moieties exists, it is possible to predict through computational calculations the structure of the derived coordination compounds. Based on the structural arrangement of a set of camphor sulfonimines, some insights into the structural arrangement of several coordination compounds frameworks as well as the electronic or packing effects being predominant in the camphor sulfonimines.

2. Results and discussion

Two new coordination compounds $[\text{Ag}(\text{NO}_3)\text{L}_2]$ (**C1**: L^6 and **C2**: L^7) were synthesized (see experimental) from reaction of AgNO_3 with camphor sulfonimines: 3,5- $\text{Me}_2\text{C}_6\text{H}_3\text{C}_{10}\text{H}_{13}\text{SO}_2$ (L^6) and $\text{C}_6\text{H}_5\text{C}_{10}\text{H}_{13}\text{SO}_2$ (L^7) which enlarge the pool of $[\text{Ag}(\text{NO}_3)\text{L}_n]$ ($n=1, 2$) camphor sulfonimine complexes with potential biological applications as anticancer or antimicrobial agents.[3,10] Unfortunately, the structure of these two camphor sulfonimine $\text{Ag}(\text{I})$ complexes such as that of many others could not be confirmed by X-ray diffraction analysis since no suitable crystals could be obtained. Therefore, calculations based on X-ray data obtained for the ligands can help to get insight into the structural arrangement of the complexes. In one case, data obtained by X-rays showed that $[\text{Ag}(\text{NO}_3)\text{L}_2]$ ($\text{R}=\text{NMe}_2$) arranges as a calix (Scheme 1).[3]



Scheme 1. The packing structure of this complex (Figure 1) shows that the silver atom occupies essentially the empty space (grey polyhedral in Figure 1) in the packing imposed by the Non-Bonding Interactions (NBI) established between the organic fragments. Such observation prompts the prediction of other MOFs through superimposition of $\text{Ag}(\text{I})$ metal centres in the camphor sulfonimines organic frameworks whose structures are available from X-ray diffraction data and/or are calculated by DFT-D3.

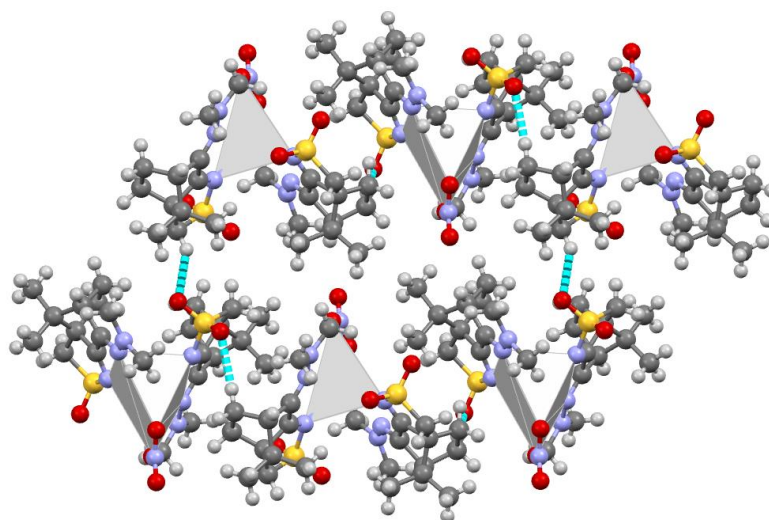
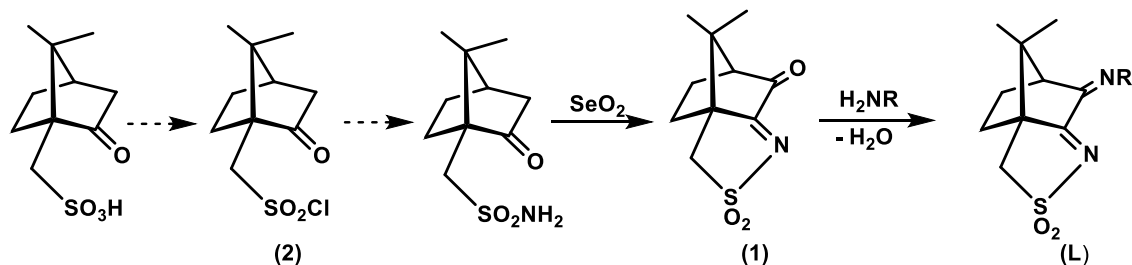


Figure 1. MOF for $[\text{Ag}(\text{NO}_3)_2\text{L}_2]$ ($\text{L}=\text{RNC}_{10}\text{H}_{13}\text{NSO}_2$; $\text{R}=\text{NMe}_2$). Grey polyhedral represents the volume occupied by the silver atom.

2.1. Synthesis of camphor sulfonylimines

The camphor sulfonylimine compounds ($\text{RNC}_{10}\text{H}_{13}\text{NSO}_2$: L^1 , $\text{R}=\text{OH}$; L^2 , $\text{R}=4\text{-OHC}_6\text{H}_4$; L^3 , $\text{R}=4\text{-NH}_2\text{C}_6\text{H}_4$; L^4 , $\text{R}=4\text{-ClC}_6\text{H}_4$; L^5 , $\text{R}=4\text{-CH}_3\text{C}_6\text{H}_4$; L^6 , $\text{R}=3,5\text{-(CH}_3)_2\text{C}_6\text{H}_3$; L^7 , $\text{R}=\text{C}_6\text{H}_5$) were obtained by condensation (Scheme 2, right) of the convenient primary amine (H_2NR) with (1*S*)-3-oxo-camphorsulfonyl imine (**1**). Precursor **1** was obtained from camphor sulfonic acid through a sequential process that involves formation of compound **2** (Scheme 2, left) and ends on the oxidative annulation of a third ring the bicyclic camphor precursor.



Scheme 2. $\text{R}=\text{OH}$, L^1 ; $\text{R}=4\text{-OHC}_6\text{H}_4$, L^2 ; $\text{R}=4\text{-NH}_2\text{C}_6\text{H}_4$, L^3 ; $\text{R}=4\text{-ClC}_6\text{H}_4$, L^4 ; $\text{R}=4\text{-CH}_3\text{C}_6\text{H}_4$, L^5 ; $\text{R}=3,5\text{-(CH}_3)_2\text{C}_6\text{H}_3$, L^6 ; $\text{R}=\text{C}_6\text{H}_5$, L^7 .

From the camphorimine species under study ($\text{L}^1\text{--L}^7$), four are new (L^1 , L^2 , L^4 and L^6) and were characterized by conventional analytical and spectroscopic techniques (FT-IR, ^1H NMR, ^{13}C NMR and 2D NMR). The remaining compounds were just recrystallized to obtain single crystals. The structural arrangement of all compounds was then studied by X-ray diffraction analysis. Based on the X-ray data, the *intra* and *inter* molecular NBI were predicted by DFT-D3. Therefore, the supramolecular arrangement of compounds **1**, **2** and the camphor sulfonylimines $\text{L}^1\text{--L}^7$ was elucidated.

2.2. Structural arrangement predicted by DFT-D3

Compounds 1 and 2

The X-ray data obtained for compound **1** indicates that a 3D helicoidal packing exists around the 3_1 crystallographic axes due to non-conventional oxygen...hydrogen (aliphatic) NBI (Figure 1a). DFT-D3 calculations, performed in a subset dimer of **1**, confirm the observed NBI and predict them

as even stronger than those experimentally observed by X-ray analysis, as illustrated by shorter distances (Figure 2b).

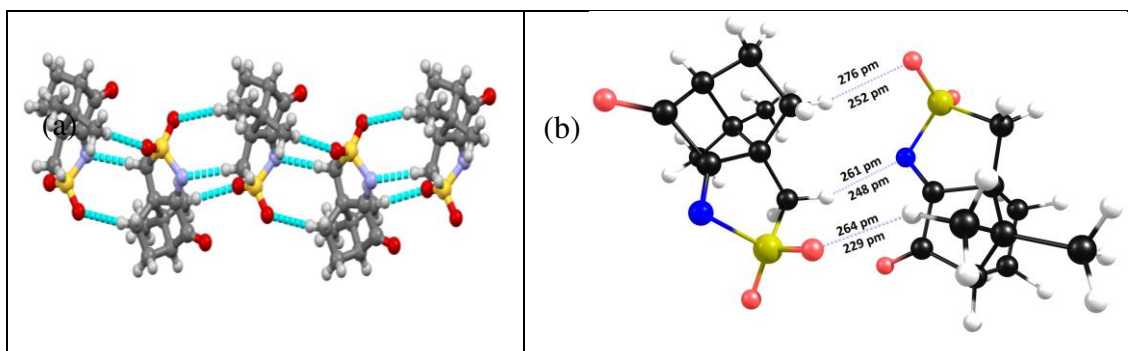


Figure 2. (a) X-ray diffraction data showing the helicoidal packing for **1**; (b) - NBI lengths according to X-ray data (above) and DFT-D3 calculations on a subset dimer of **1**.

For **2**, calculations were based on the X-ray data reported by others.[11] The X-ray shows a zig-zag 1D structural arrangement due to chloride-oxygen intermolecular NBI established by the pendant sulphonyl chloride (SO_2Cl) groups in adjacent molecules (Figure 3). Such type of cooperative intermolecular $\text{S}-\text{Cl}\cdots\text{O}$ interaction was previously discussed[12] on the basis of the $\text{S}-\text{Cl}\cdots\text{O}$ and $\text{S}-\text{O}\cdots\text{Cl}$ angles (θ) and classified (Figure 3, insert) as type I ($\theta_1=\theta_2$) or type II ($\theta_1=180^\circ$, $\theta_2=90^\circ$).[13]

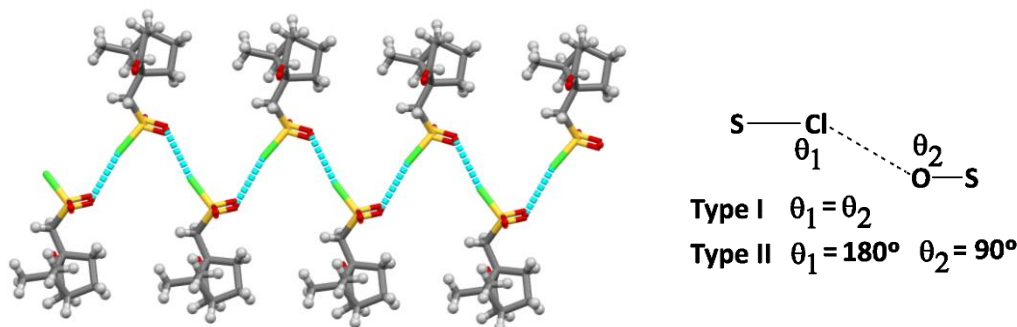


Figure 3. Drawing evidencing the bi-dimensional intermolecular interactions in **2**.

Such as for **1**, DFT-D3 calculations for **2** were carried out in a subset dimer of the structural arrangement found by X-ray diffraction analysis. Once more, the output data shows good agreement between experimental and calculated values (Table 1), in agreement with the electrostatic directionality of the interactions.

Table 1. Intermolecular interactions in **2** (distances pm; angles deg).

Parameter	X-Ray	DFT-D3	NBI quasi-Type II
$\text{Cl}\cdots\text{O}$	300	311	
$\text{S}-\text{Cl}\cdots\text{O}$	169.4	176.4	
$\text{S}-\text{O}\cdots\text{Cl}$	131.5	128.2	

2.3. Camphor sulfonylimines (L^1 - L^7)

The X-ray data collected for the sulfonylimine compounds L^1 to L^7 show different packing motives according to the imine substituent (R). In L^1 ($\text{R}=\text{OH}$) the asymmetric unit is formed by two structurally different molecules as shown in Figure 4 (center) since chirality prevents the existence of an inversion center.

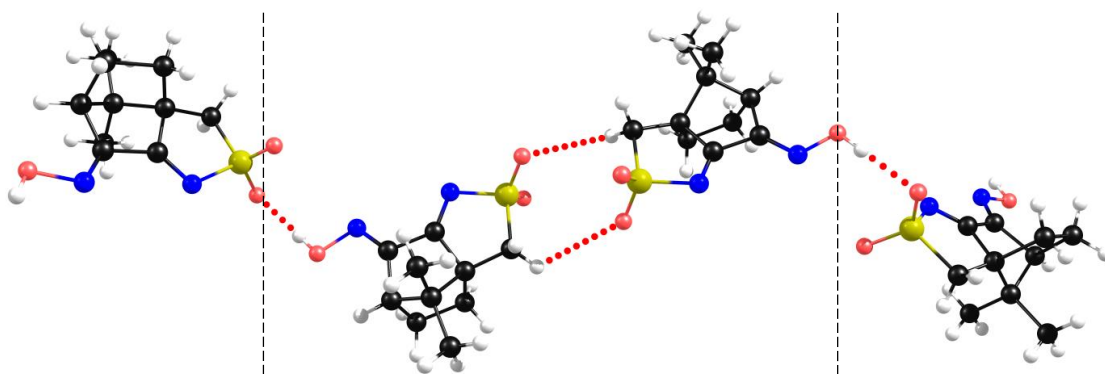


Figure 4. X-Ray packing for L^1 . The central dimer is the asymmetric unit composed by two different molecules.

The X-ray data, shows that at the “dimeric” asymmetric unit, the NBI are type I ($\theta_1 = \theta_2$, *i.e.* $S-O \cdots H=C-H \cdots O = 108^\circ$) while the NBI established between neighbor asymmetric units (involving the sulfonimine oxygen atom and the hydrogen hydroxyl atom) are of type II ($\theta_1 \neq \theta_2$, *i.e.* $S-O \cdots H = 109^\circ$ and $O-H \cdots O = 171^\circ$). The DFT-D3 calculations corroborate the type II nature of this NBI (Figure 5, left) but in what concerns the asymmetric unit DFT-D3 calculations predict type II NBI (Figure 5, right) in contrast with experimentally observed by X-ray diffraction. Such results indicate that NBI type I experimentally observed are due to packing constraints rather than to electrostatic effects.

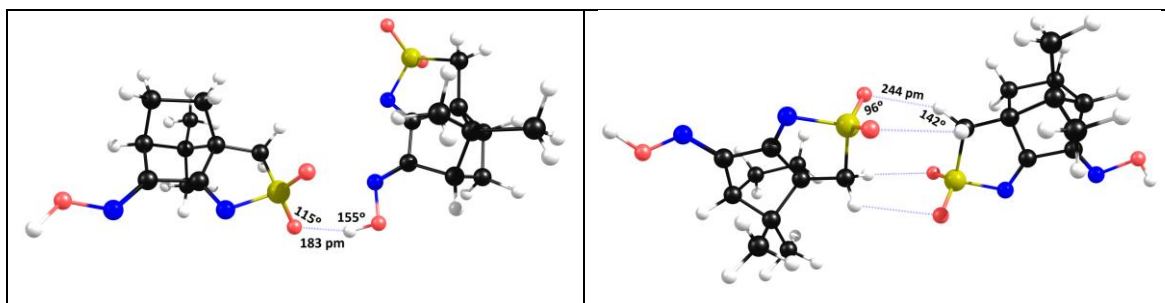


Figure 5. Data obtained by DFT-D3 for the NBI's in the hydroxyl (left) and central dimer (right) in L^1 .

From Figures 4 and 5, it comes out that the asymmetric unit remains unchanged both experimental and in DFT-D3 calculations with the two nitrogen atoms not involved in NBI and thus available for complexation with the metal center $AgNO_3$. The introduction of the metal center in the calculations (Figure 6) confirms that a MOF can form through coordination of the cyclic imine nitrogen atom to the metal, keeping the 1D chain of the organic framework (OF).

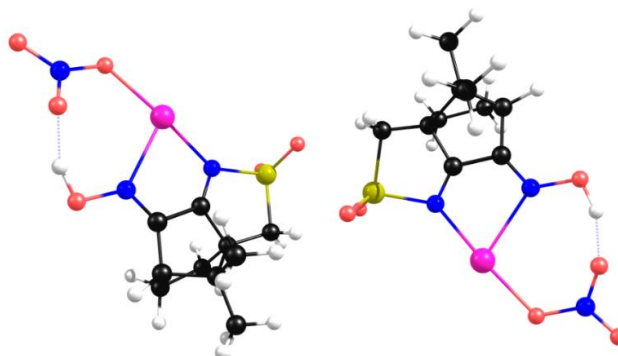


Figure 6. Prediction by DFT-D3 of the structural arrangement of $[AgNO_3L^1]$.

Camphor sulfonimine compounds with aromatic substituents (R, Scheme 2) at the imine group (L^2 to L^7), display self-assembly behaviors quite different from L^1 (R=OH).

A 1D assembly exists in **L**⁴ (R=4-ClC₆H₄), **L**⁵ (R=4-CH₃C₆H₄), **L**⁶ (3,5-(CH₃)₂C₆H₄) and **L**⁷ (R=C₆H₅) which is formed by non-conventional NBI established between the nitrogen atom of the -SO₂N- group and one of the hydrogen atoms of the methylene (CH₂) group of the five membered sulfonimine ring of a neighbor molecule. As a representative example, the X-ray diffraction data is displayed for **L**⁷ (Figure 7, left). The results from the DFT-D3 calculations agree well with the experimental obtained X-rays data (Figure 7, right). Such as for **1** the predicted NBI distances are shorter than the experimentally measured pointing to stronger electronic interactions.

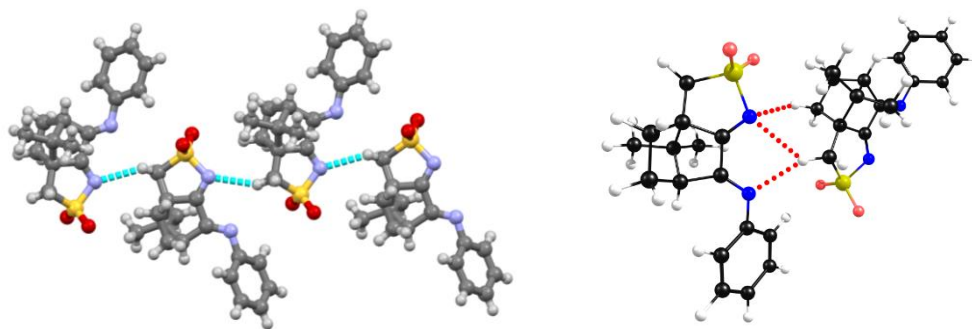


Figure 7. Structural arrangement for **L**⁷: X-Ray data (left) showing 1D assembly through a N...H-C NBI and DFT-D3 optimized structure (right).

In the aromatic substituted camphor sulfonimines (**L**⁴ to **L**⁷) the cyclic nitrogen imine atom of the 1D organic framework is involved in NBI which means that complexation would break down the self-assembly trends observed in the OF. So, MOFs are expected to have different frameworks than those observed in the ligands **L**⁴ to **L**⁷.

At the camphor sulfonimines bearing a protic substituent (R=OH in **L**² or R=NH₂ in **L**³) at the -NR imine group (Scheme 2), the characteristics of the NBI differ from those observed for **L**⁴-**L**⁷. In **L**² and **L**³ the NBI are of the stacking π - π type, established between the aromatic carbon atoms of two distinct asymmetric units occupying the *ortho* positions relative to the heterogeneous (N or O) atoms, as depicted for **L**² (Figure 8, left). In **L**² and **L**³ NBI involving the sulfonyl imine group (not observed for **L**⁴-**L**⁷) are established by a symmetry related chain of molecules (Figure 8, left). These additional interactions were included in the DFT-D3 calculations (Figure 8, right) to get consistency between X-ray and calculated structures. Here again, such as for **L**¹ the two nitrogen imine atoms are free to complex the AgNO₃ metal center to form a MOF mimicking the self-assembly characteristics of the corresponding OF.

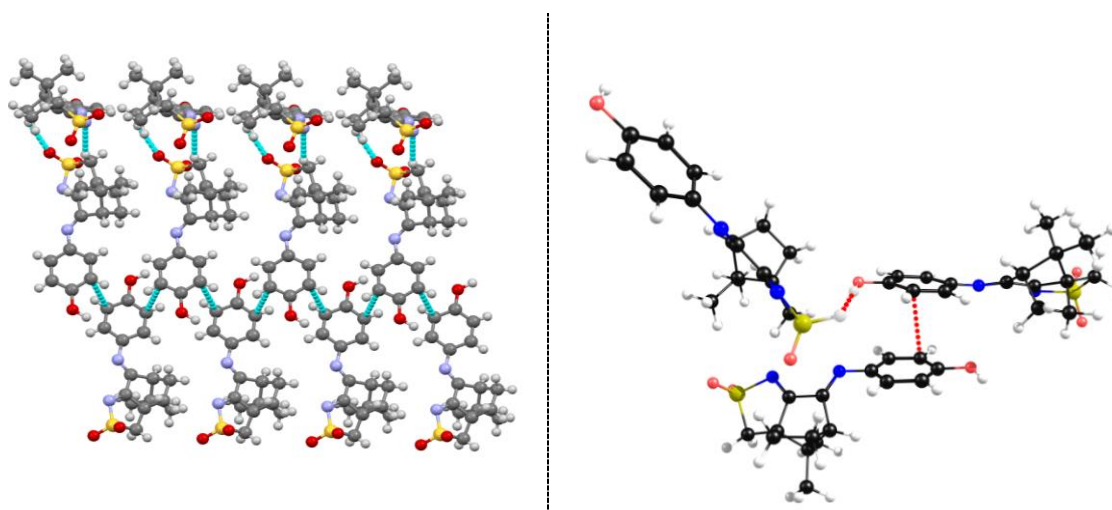


Figure 8. X-Ray data (left) showing the π - π stacking in **L**²; structure optimization made by DFT-D3 (right).

2.4. Redox properties

Packing and electronic parameters have distinct effects on the properties of the molecules. While the electronic characteristics persist no matter the physical state (solid or solution), packing essentially drives the solid-state properties.

The above results show that the structural arrangement in camphor sulfonimines (**L**²-**L**⁷) and in compounds **1** and **2** is essentially directed by electronic parameters. In contrast, packing plays an important role in the supramolecular arrangement of **L**¹, by imposing a type I NBI geometry (see above).

In order, to get insights whether a correlation exists between the structural parameters and the redox potentials and try to ascertain whether NBI interactions remain in solution, the electrochemical behavior of the **L**¹-**L**⁷ compounds was studied by cyclic voltammetry.

In acetonitrile, compounds **L**¹-**L**⁷ display one irreversible anodic wave and one (**L**¹, **L**², **L**⁵, **L**⁶, **L**⁷) or two (**L**³, **L**⁴) cathodic waves (Figure 9). In the case there are two cathodic waves, the higher potential wave (I) typically displays a higher intensity than the lower potential one (wave II). The reversibility of wave I decreases upon scan at the potential of wave II as shown (Figure 9, left). The loss of reversibility and emergence of the anodic wave X is consistent with chemical reactivity being induced by electron transfer.

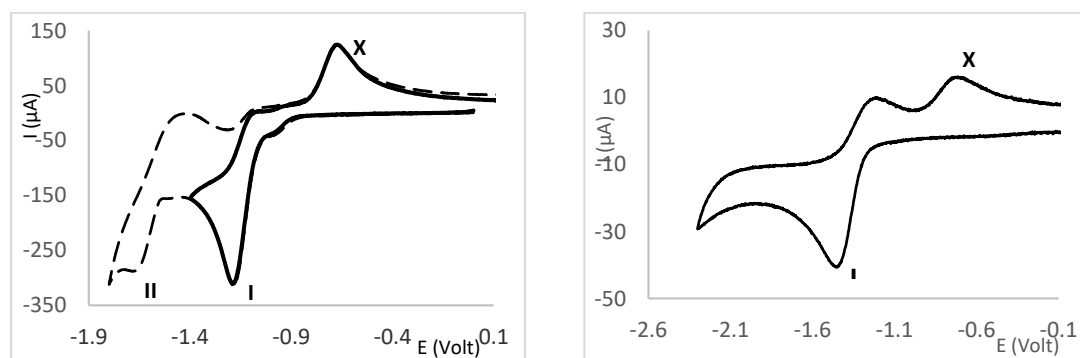
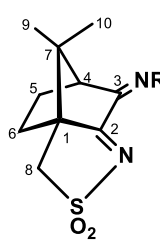


Figure 9. –Cyclic voltammograms obtained in Bu₄NBF₄/CH₃CN at 200 mV/s: **L**⁴(left) - - - full cathodic scan; — partial scan reversed after wave I; **L**⁵ (right).

The anodic and cathodic potentials measured for **L**¹- **L**⁷ are displayed in Table 2.

Table 2. - Cyclic voltammetry data^a for camphor sulfonimine compounds **L**¹– **L**⁷.

R			^I E _{1/2} ^{red}	^{II} E _p ^{red}	E _p ^{ox}	σ _p ^b
			Volt			
	OH	L ¹	-1.03	—	—	0.12
	4-OHC ₆ H ₄	L ²	-1.35	—	1.25	-0.37
	4-NH ₂ C ₆ H ₄	L ³	-1.24	-1.69	0.87	-0.66
	4-ClC ₆ H ₄	L ⁴	-1.08	-1.61	—	0.23
	4-CH ₃ C ₆ H ₄	L ⁵	-1.25	—	1.80	-0.17
	3,5-(CH ₃) ₂ C ₆ H ₃	L ⁶	-1.15	—	1.80	0.017
	C ₆ H ₅	L ⁷	-1.16	—	—	0

^a Values in Volt ±10 mV, versus SCE using ferrocene as internal reference.

The potential trend observed for wave I (Table 2) suggests that reduction involves the imine >C=N-R group. In fact, an excellent correlation exists (Figure 10, left) between the redox potential and the Hammett sigma parameter (σ_p) [14] which accounts for the electronic characteristics of the R group driving the cathodic process. Compounds **L**¹ (R=OH) and **L**³ (4-NH₂C₆H₄) are aside from the linear correlation (R²=0.987) established by the other compounds showing that other than electronic parameters operate.

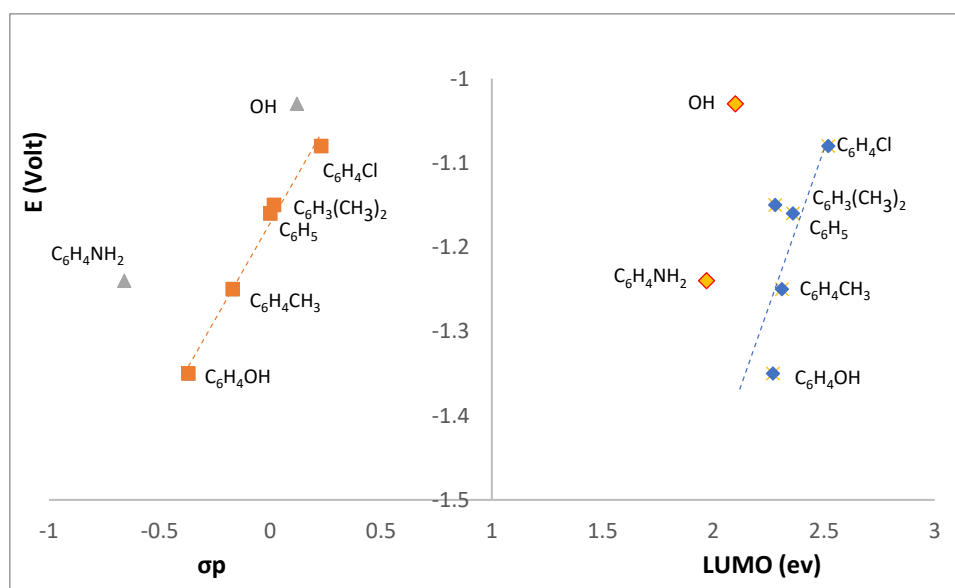


Figure 10. Correlation between the reduction potential ($E_{1/2}^{red}$) of L^1 - L^7 and the Hammett parameter (σ_p) or LUMO (right).

In what concerns L^1 such behavior was somehow expected due to the non-aromatic character of the R group (unlike the R groups at L^2 - L^7) and the distinct type of NBI (see DFT-D3 discussion, above) compared to the other compounds.

In what concerns the relationship between $E_{1/2}^{red}$ and the LUMO (Figure 10, right) the energy calculations for L^1 show that there is a decrease by 0.11 eV in the absolute value of the energy in the H-bonded dimer. Such energy shift may account for the non-fitting of the potential (FIGURE 10, right) pointing to L^1 keeping some dimer character in the electrolyte solution.

L^3 is the other compound that does not fit the $E_{1/2}^{red}$ versus σ_p (Figure 10, left) neither fits the $E_{1/2}^{red}$ versus LUMO (Figure 10, right) correlations. The two compounds (L^1 , R=OH and L^3 , R= $C_6H_4NH_2$) have in common the protic character of the R imine substituent which induces formation of H-bonded dimers (see above).

In what concerns the anodic behavior, just L^2 , L^3 , L^5 and L^6 show oxidation processes. L^2 and L^3 display the lowest oxidation potentials in agreement with the electron releasing characteristics of the aromatic R groups as corroborated through the linear correlation with Hammett σ_p parameters (Figure 11, left). A good correlation with the HOMO was found (Figure 11, right).

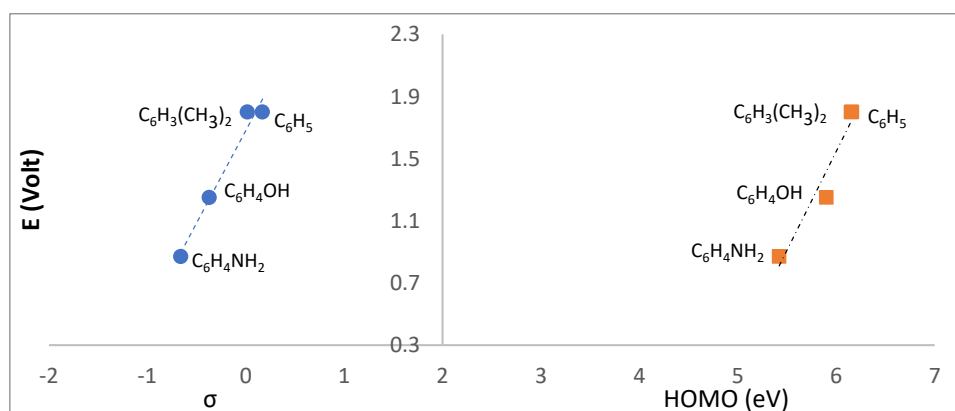


Figure 11. Relationship between the Hammett parameters (σ_p) and the oxidation potentials measured for the camphor sulfonylmines.

The calculated HOMO and LUMO contours for compound **L7** show that the HOMO is mostly localized at the aromatic ring (all carbons) while the LUMO is localized at the camphor skeleton with an important contribution from the 2, 4 and 6 ring carbon atoms (Figure 12).

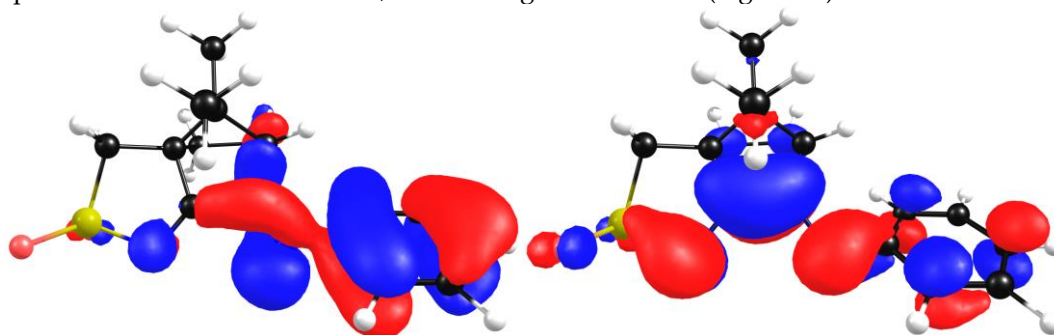


Figure 12. Wavefunction contours for HOMO (left) and LUMO (right) for **L7**.

The electrochemical behavior of $[\text{Ag}(\text{NO}_3)_2\text{L}_2]$ (**C1**, **C2**) complexes studied by cyclic voltammetry show that a cathodic process exists at a potential ($E_p^{\text{red}} = -1.18$ V, **C1** and $E_p^{\text{red}} = -1.17$ V, **C2**) similar to that measured for the organic precursors **L6** and **L7**, respectively (Table 2). Such pattern indicate that the electronic properties of the sulfonimine ligands remain essentially identical in the complexes. As expected, the cyclic voltammograms of **C1** and **C2** display a cathodic wave attributed to the $\text{Ag}(\text{I}) \rightarrow \text{Ag}(0)$ reduction at a potential ($E_p^{\text{red}} = 0.16$ V) that does not differ much of that reported for related complexes.[3]

The redox behavior of **1** was also studied by cyclic voltammetry showing a *quasi*-reversible cathodic wave ($E_{1/2}^{\text{red}} = -0.92$ V; $\text{ipc}/\text{ipa} = 1$, $E_{\text{pa}} - E_{\text{pc}} = 133$ mV) but no anodic process. According to the cathodic potential value, reduction of **1** is easier than any of the sulfonimine compounds (**L1-L7**, Table 1). Therefore, sulfonimines are more electron rich than **1** and consequently better ligands for metal sites. In fact, no $\text{Ag}(\text{I})$ complex based on **1** could be experimentally obtained, in contrast with several complexes derived from sulfonimine ligands as for example the new $[\text{Ag}(\text{NO}_3)_2\text{L}_2]$ (**C1** and **C2**) now reported (see experimental).

3. Conclusions

DFT-D3 calculations based on X-ray data obtained for a series of camphor sulfonimine compounds corroborate that NBI are responsible for their organic framework. On $^2\text{L-}^7\text{L}$ the NBI are essentially electrostatic, in contrast with ^1L where packing plays a relevant role in the solid-state arrangement observed by X-rays analysis.

The characteristics of the sulfonimine substituent (R) fine drives the NBI established and direct the ability of the **L** compounds to bind the $\text{Ag}(\text{I})$ metal center forming MOFs such as detected for $[\text{Ag}(\text{NO}_3)(\text{O}_2\text{SNC}_{10}\text{H}_{13}\text{NNMe}_2)_2]$ whose X-ray structure was formerly reported.

It was found that complexation of the metal center always occurs in a monodentate fashion through the imine nitrogen atom in the sulphonyl 5-membered ring. It was predicted by DFT-D3 calculations that the NBI interactions not involving this atom remain after complexation being transferred to the MOF. The conjugation of the x-ray structures of the organic ligands with DFT-D3 calculations proved to be a powerful tool to predict the self-assembly trends of the corresponding MOF structures of the complexes.

The correlation between the redox potentials of $^1\text{L-}^7\text{L}$ (studied by cyclic voltammetry), the Hammett σ -parameter and calculated HOMO and LUMO energies are in excellent agreement with different types of NBI being established by ^1L and ^2L compared to the other camphor sulfonimine compounds.

4. Experimental

The camphor sulfonimines **L**¹, **L**³, **L**⁵ and **L**⁷ were synthesized according to published procedures.[15] The complexes were synthesized under nitrogen using Schlenk and vacuum techniques. The FT-IR spectra were obtained from KBr pellets using a JASCO FT/IR 4100 spectrometer. The NMR spectra (¹H, ¹³C, DEPT, HSQC, and HMBC) were obtained from CDCl₃, CD₃CN or DMSO solutions using Bruker Avance II+ (300 or 400 MHz) spectrometers. The NMR chemical shifts are referred to TMS ($\delta=0$ ppm).

The redox properties were studied by cyclic voltammetry using a three compartments cell equipped with Pt wire electrodes (work and secondary) and interfaced with a VoltaLab PST050 equipment. The cyclic voltammograms were obtained from NBu₄BF₄ / CH₃CN (0.10 M) solutions used as electrolyte. The potentials were measured in Volts (± 10 mV) *versus* SCE at 200 mV/s using [Fe(η^5 -C₅H₅)₂]^{0/+} ($E_{1/2}^{ox} = 0.382$ V; CH₃CN) as internal reference. The window of potential was established by scanning a fresh solution of the electrolyte to the limits.

4.1. Synthesis

4.1.1. Camphor sulfonimines

(*E*)-7-(hydroxyimino)-8,8-dimethyl-4,5,6,7-tetrahydro-3H-3a,6-ethanobenzo[c] isothiazole 2,2-dioxide (**L**¹) - Compound **1** (682 mg; 3 mmol) was dissolved in ethanol (10 mL) acidified with acid acetic (0.4 mL) and the mixture was stirred for *ca.* 15 minutes before the hydroxylamine (99 mg, 3 mmol) was added. The reaction was stopped after 24 hours stirring by addition of 5 mL of water. The organic phase was then extracted with dichloromethane (3x5 mL) and dried over MgSO₄ for a couple of hours. After filtration the solvent was allowed to evaporate slowly in the exhaust hood. Yield 71%. Elem. Anal. (%) for C₁₀H₁₄N₂O₃S: Found: C, 49.8; N, 11.3; H, 6.0; S, 13.7. Calc.: C, 49.6; N, 11.6; H, 5.8; S, 13.2. FTIR (KBr, cm⁻¹): 3367, 1668, 1633, 1327, 1158. ¹H NMR (DMSO, δ ppm): 12.8 (s, 1H); 3.59, 3.36 (2d, $J=14.0$ Hz, 2H); 3.25 (d, $J=4.2$ Hz, 1H); 2.22 – 2.01 (m, 2H); 1.63 – 1.40 (m, 2H); 1.01 (s, 3H); 0.78 (s, 3H). ¹³C NMR (DMSO, δ ppm): 184.7, 155.3, 64.2, 49.0, 47.9, 47.1, 28.8, 23.6, 19.5, 18.1.

(*E*)-7-((4-hydroxyphenyl)imino)-8,8-dimethyl-4,5,6,7-tetrahydro-3H-3a,6-methanobenzo[c]isothiazole 2,2-dioxide (**L**²) - 3-oxo-camphorsulfonimide (**1**, 682 mg; 3 mmol) was dissolved in ethanol (10 mL) acidified with CH₃COOH (0.4 mL). The mixture was stirred for 15 minutes before adding the 4-aminophenol (329 mg; 3 mmol). A light brown compound was formed upon overnight stirring at 50°C that was filtered off the solution and dried. Yield 81%. Elem. Anal. (%) for C₁₆H₁₈N₂O₃S·H₂O: Found: C, 56.9; N, 8.0; H, 6.2; S, 11.1. Calc.: C, 57.1; N, 8.3; H, 6.0; S, 9.5. FTIR (KBr, cm⁻¹): 3567, 1653, 1633, 1330, 1160. ¹H NMR (CD₃CN, δ_{ppm}): 7.35 (s, 1H, OH), 7.00 (d, $J=7.8$ Hz, 2H), 6.88 (d, $J=7.8$ Hz, 2H), 3.48, 3.25 (2d, $J=13.9$ Hz, 2H), 3.10 (d, $J=2.6$ Hz, 1H), 2.34–2.23 (m, 2H), 1.89–1.75 (m, 2H), 1.06 (s, 3H), 0.84 (s, 3H). ¹³C NMR (CD₃CN, δ_{ppm}): 187.9, 166.0, 157.3, 141.9, 124.9, 116.7, 64.1, 52.6, 50.5, 47.8, 29.4, 24.4, 19.9, 18.3.

(*E*)-7-((4-chlorophenyl)imino)-8,8-dimethyl-4,5,6,7-tetrahydro-3H-3a,6-methanobenzo[c]isothiazole 2,2-dioxide (**L**⁴) - Compound **1** (682 mg; 3 mmol) was dissolved in acidified (acid acetic, 0.4 mL) ethanol (10 mL) and stirred for *ca.* 15 minutes. Upon addition of 4-chloroaniline (384 mg, 3 mmol) the reaction was stirred overnight at 40°C. A yellow precipitate formed that was filtered off solution and dried. Yield 76%. Elem. Anal. (%) for C₁₆H₁₇ClN₂O₂S·1/5H₂O: Found: C, 56.5; N, 8.1; H, 5.3; S, 10.1. Calc.: C, 56.5; N, 8.2; H, 5.2; S, 9.4. FTIR (KBr, cm⁻¹): 1664, 1636, 1340, 1161. ¹H NMR (CDCl₃, δ ppm): 7.39 (d, $J=8.6$ Hz, 2H); 6.93 (d, $J=8.6$ Hz, 2H); 3.42, 3.21 (2d, $J=13.4$ Hz, 2H); 2.99 (d, $J=8.6$ Hz, 1H); 2.29 – 2.21 (m, 2H); 2.10 – 2.00 (m, 1H); 1.82 – 1.74 (m, 1H); 1.11 (s, 3H); 0.95 (s, 3H). ¹³C NMR (CDCl₃, δ_{ppm}): 185.0, 167.5, 147.2, 132.1, 129.4, 122.0, 62.7, 51.4, 50.0, 46.8, 28.4, 24.1, 20.0, 18.4.

(*E*)-7-((3,5-dimethylphenyl)imino)-8,8-dimethyl-4,5,6,7-tetrahydro-3H-3a,6-methanobenzo[c]isothiazole 2,2-dioxide (**L**⁶) - Compound **1** (454 mg; 2 mmol) was dissolved in ethanol (7 mL) acidified with acid acetic (0.2 mL) and the mixture stirred for *ca.* 15 minutes. Then, 3,5-dimethylaniline (0.25 mL, 2 mmol) was added and the reaction stirred for 24 hours at RT. A brown precipitate formed that was filtered off solution and dried. Yield 86%. Elem. Anal. (%) for C₁₈H₂₂N₂O₂S: Found: C, 65.3; N, 8.4; H, 6.7; S, 9.5. Calc.: C, 65.4; N, 8.5; H, 6.7; S, 9.7. FTIR (KBr, cm⁻¹):

1665, 1636, 1339, 1161. ^1H NMR (CDCl_3 , δ ppm): 6.87 (s, 1H); 6.56 (s, 2H); 3.39, 3.18 (2d, J = 13.4 Hz, 1H); 3.01 (d, J = 4.0 Hz, 1H); 2.34 (s, 6H); 2.24 – 2.19 (m, 2H); 2.05 – 1.98 (m, 1H); 1.82 – 1.75 (m, 1H); 1.09 (s, 3H); 0.94 (s, 3H). ^{13}C NMR (CDCl_3 , δ ppm): 185.4, 166.5, 149.1, 139.1, 128.1, 118.2, 113.6, 62.9, 51.5, 50.1, 46.8, 28.6, 24.3, 21.5, 21.4, 20.1, 18.5.

4.1.2. Complexes

[$\text{Ag}(\text{NO}_3)\{(\text{3,5-Me}_2\text{C}_6\text{H}_3)\text{NC}_{10}\text{H}_{13}\text{NSO}_2\}_2$] (**C1**) – AgNO_3 (42.5 mg; 0.25 mmol) was added to a solution of **L**⁶ (165 mg; 0.50 mmol) in CH_3CN (5 mL) and the mixture was stirred for 2 hours. A light suspension formed that was filtered to separate silver residues. The filtered solution was evaporated and dried under vacuum to afford **C**₁ as a dark yellow compound. Yield 72%. Elemental analysis for $\text{AgC}_{36}\text{H}_{44}\text{N}_5\text{O}_7\text{S}_2 \cdot 1/5\text{HNO}_3$ Exp.: C, 51.2; N, 8.4; H, 5.5; S, 8.8. Calc.: C, 51.3; N, 8.6; H, 5.3; S, 7.6. FTIR (KBr, cm^{-1}): 1666, 1644, 1384, 1338, 1161. ^1H NMR (400 MHz, CD_3CN , δ ppm): 6.91 (s, 1H); 6.59 (s, 2H); 3.51, 3.28 (2d, J =14 Hz, 2H); 2.96 (d, J =4.8 Hz, 1H); 2.31 (s, 6H); 2.24 – 2.30 (m, 1H); 1.71 – 1.88 (m, 3H); 1.05 (s, 3H); 0.87 (s, 3H). ^{13}C NMR (400 MHz, CD_3CN , δ ppm): 186.5, 167.7, 149.2, 139.2, 127.6, 117.8, 63.2, 51.4, 49.7, 46.5, 28.0, 23.6, 20.3, 19.1, 17.1.

[$\text{Ag}(\text{NO}_3)(\text{C}_6\text{H}_5\text{NC}_{10}\text{H}_{13}\text{NSO}_2)_2$] (**C2**) - Silver nitrate (42.5 mg; 0.25 mmol) was added to a solution of **L**⁷ (151 mg; 0.50 mmol) in CH_3CN (3 mL) and the mixture stirred for 2 hours.

The suspension was then filtered to remove silver residues. Upon solvent evaporation and drying under vacuum the compound was obtained as a yellow powder. Yield 62%. Elemental analysis for $\text{AgC}_{32}\text{H}_{36}\text{N}_5\text{O}_7\text{S}_2 \cdot \text{H}_2\text{O}$ Exp.: C, 48.6; N, 9.0; H, 4.7; S, 7.6. Calc.: C, 48.5; N, 8.8; H, 4.8; S, 8.1. FTIR (KBr, cm^{-1}): 1664, 1635, 1384, 1346, 1165. ^1H NMR (400 MHz, DMSO, δ ppm): 7.46 (t, J =15.7 Hz, 2H); 7.25 (t, J =7.4 Hz, 1H); 7.00 (d, J =8.4 Hz, 2H); 3.74, 3.52 (2d, J =14 Hz, 2H); 2.88 (d, J =4.8 Hz, 1H); 2.34–2.25 (m, 1H); 2.19–2.10 (m, 1H); 1.80–1.70 (m, 2H); 1.01 (s, 3H); 0.84 (s, 3H). ^{13}C NMR (400 MHz, DMSO, δ ppm): 186.0, 167.8, 148.8, 129.3, 126.0, 120.1, 63.0, 51.0, 49.3, 46.3, 27.7, 23.4, 19.2, 17.5.

4.2. Computational methods

All theoretical calculations were of the DFT type, carried out using GAMESS-US version R3,[16] using the implemented version of the B3LYP functional and a 6-31G** basis set for organic molecules and SBKJC basis set/ECP in metal complexes. DFT-D3[17] with the standard parametrization of GAMESS-US, was used in all computational work. Optimized geometries were confirmed to be minima by checking for absence of imaginary frequencies in the Hessian.

4.3. X-ray diffraction analysis

X-ray diffraction analysis was performed on mono crystals of **1,3** and **L1** to **L7**. Data was collected on a Bruker AXS-KAPPA APEX II area detector apparatus using graphite-monochromated Mo K α (λ =0.71073 Å) and were corrected for Lorentz, polarization and empirically for absorption effects. The structure was solved by direct methods using SHELX97[18] and refined by full matrix least squares against F^2 using SHELX97 all included in the suit of programs WinGX v1.70.01 for Windows.[19] Non-hydrogen atoms were refined anisotropically and H atoms were inserted in idealized positions and allowed to refine riding on the parent carbon atom. Crystal data and refinement parameters are summarized in Table 3. Illustrations of the molecular structures were made with Chemcraft[20] or Mercury.[21]

CCDC 2252538 to 2252543 and CCDC 2252556 contain the supplementary crystallographic data for this paper which can be obtained free of charge via www.ccdc.cam.ac.uk/conts/retrieving.html (or from the Cambridge Crystallographic Data Centre, 12, Union Road, Cambridge, CB2 1EZ, UK; fax: +44 1223 336033; or deposit@ccdc.cam.ac.uk).

Table 3. Crystallographic data for **1** and **L**¹ to **L**⁴, **L**⁶, **L**⁷.

	1.	L ¹	L ⁴	L ⁶	L ⁷
Empirical formula	$\text{C}_{10}\text{H}_{13}\text{NO}_3\text{S}$	$\text{C}_{20}\text{H}_{28}\text{N}_4\text{O}_6\text{S}_2$	$\text{C}_{16}\text{H}_{17}\text{ClN}_2\text{O}_2\text{S}$	$\text{C}_{18}\text{H}_{22}\text{N}_2\text{O}_2\text{S}$	$\text{C}_{16}\text{H}_{18}\text{N}_2\text{O}_2\text{S}$
Formula weight	227.27	484.58	336.83	330.43	302.38

Crystal system	Tetragonal	Monoclinic	Orthorhombic	Orthorhombic	Orthorhombic
Space group	P4 ₃ 2 ₁ 2	P2 ₁	P2 ₁ 2 ₁ 2 ₁	P2 ₁ 2 ₁ 2 ₁	P2 ₁ 2 ₁ 2 ₁
Unit cell dim.					
a/ Å	7.6255(5)	6.9975(4)	8.8877(6)	9.121(2)	9.375(1)
b/ Å	7.6255(5)	13.9378(9)	12.0522(7)	11.174(2)	11.724(1)
c/ Å	36.400(2)	11.3550(7)	14.9100(6)	35.256(6)	14.130(2)
α/ deg	90	90	90	90	90
β/ deg	90	95.520(3)	90	90	90
γ/ deg	90	90	90	90	90
Volume (Å ³)	2116.6(2)	1102.3(1)	1597.1(2)	3593(1)	1553.1(3)
Z, Dcal (g/cm ³)	8, 1.426	2, 1.460	4, 1.401	8, 1.222	4, 1.293
Abs. coeff. (mm ⁻¹)	0.292	0.288	0.378	0.191	0.214
F(000)	960	512	704	1408	640
Crystal size (mm ³)	0.3 x 0.3 x 0.3	0.3 x 0.3 x 0.3	0.2 x 0.1 x 0.1	0.4 x 0.3 x 0.2	0.2 x 0.2 x 0.3
θ range (deg)	2.24 to 29.85	2.32 to 32.71	2.17 to 26.37	1.912 to 32.016	2.257 to 32.178
Refl. Collect./ uni.	12072 / 3022	16791 / 7667	7174 / 3253	220676 / 12299	12152 / 5275
	[R(int) = 0.0486]	[R(int) = 0.0347]	[R(int) = 0.0349]	[R(int) = 0.5558]	[R(int) = 0.0361]
Data/restr./par.	3022 / 0 / 138	7667 / 1 / 301	3253 / 0 / 199	12299 / 0 / 423	5275 / 0 / 192
Final R (observed)	R1 = 0.0342, wR2 = 0.0896	R1 = 0.0334, wR2 = 0.0865	R1 = 0.0409, wR2 = 0.1026	R1 = 0.0756, wR2 = 0.1551	R1 = 0.0438, wR2 = 0.1055

Acknowledgments: FCT - Fundação para a Ciência e a Tecnologia, for financial support through projects CQE (UIDB/00100/2020, UIDP/00100/2020) and Institute of Molecular Sciences (LA/P/0056/2020) and a PhD Grant to Joana Costa (UI/BD/152244/2021). The Portuguese NMR IST-UL Centers for facilities.

References

1. M.F.N.N. Carvalho, A.C. Consiglieri, M.T. Duarte, A.M. Galvão, A.J.L. Pombeiro, R. Herrmann, Transition metal complexes of (1S,2S,3S)-3-hidroxy-camphorsultam, *Inorg.Chem.* **1993**, 32, 5160-5164.
2. M.F.N.N. Carvalho, L.M.G. Costa, A.J.L. Pombeiro, A. Schier, W. Scherer, S.K. Harbi, U. Verfürth, R. Herrmann, Synthesis, structure and electrochemistry of palladium complexes with camphor-derived chiral ligands *Inorg. Chem.* **1994**, 33, 6270-77. doi: 10.1021/ic00104a042.
3. J.M.S. Cardoso, I. Correia, A.M. Galvão, F. Marques, M.F.N.N. Carvalho *J. Inorg. Biochem.* **2017**, 166, 55-63.
4. Y.-N. Wang, L.-Q. Lu, W.-J. Xiao, *Chem. Asian J.* **2018**, 13, 2174-2183.
5. L. Wang, S. Gou, Y. Chen, Y. Liu, *Bioorg. Med. Chem. Lett.* **2005**, 15, 3417-3422.
6. V. Rashidi, E.J. Coyle, K. Sebeck, J. Kieffer, K.P. Pipe, *J. Phys. Chem. B* **2017**, 121, 4600-4609.
7. M.F.N.N. Carvalho, S. Leite, J.P. Costa, A.M. Galvão, J.H. Leitão, *J. Inorg. Biochem* **2019**, 199, 110791.
8. T.A. Fernandes, F. Mendes, A.P.S. Roseiro, I. Santos, M.F.N.N. Carvalho, *Polyhedron*, **2015**, 87, 215-219.
9. T.A. Fernandes, A.M. Ferraria, A.M. Galvão, A.M. Botelho do Rego, A.C.M. Suárez, M.F.N.N. Carvalho, *J. Organometal. Chem.* **2014**, 760, 186-196.
10. J.H. Leitão, S.A. Sousa, S.A. Leite, M.F.N.N. Carvalho *Antibiotics*, **2018**, 7, 65
11. H.E. Armstrong, T.M. Lowry, *J. Chem. Soc.*, **1902**, 81, 1441.
12. X. Liu, Colin D. McMillen, Joseph S. Thrasher, *New J. Chem.*, **2018**, 42, 1-4.
13. Mukherjee, S. Tothadi. G. R. Desiraju, *Acc. Chem. Res.*, **2014**, 47, 2514-2524.
14. Hansch, A. Leo, R. W. Taft, *Chem. Rev.* **1991**, 97, 165-195.
15. J.P. Costa, S.A. Sousa, A.M. Galvão, J.M. Mata, J.H. Leitão, M.F.N.N. Carvalho, *Antibiotics* **2021**, 10, 135.
16. M.W. Schmidt, K.K. Baldrige, J.A. Boatz, S.T. Elbert, M.S. Gordon, J.H. Jensen, S. Koseki, N. Matsunaga, K.A. Nguyen, S. Su, T.L. Windus, M. Dupuis, J.A. Montgomery, *J. Comput. Chem.* **1993**, 14, 1347-1363.
17. S. Grimme, J. Antony, S. Ehrlich, H. Krieg, *J. Chem. Phys.* **2010**, 132, 154104.
18. G. M. Sheldrick *SHELX-97- Programs for Crystal Structure Analysis (release 97-2)*, Institut für Anorganische Chemie der Universität, Tammanstrasse 4, D-3400 Göttingen, Germany, **1998**.
19. L. J. Farrugia, *WINGX J. Appl. Crystallogr.* **1999**, 32, 837.

20. Chemcraft - graphical software for visualization of quantum chemistry computations. <https://www.chemcraftprog.com>.
21. F. Macrae, I. Sovago, S. J. Cottrell, P. T. A. Galek, P. McCabe, E. Pidcock, M. Platings, G. P. Shields, J. S. Stevens, M. Towler and P. A. Wood, *J. Appl. Cryst.*, **2020**, 53, 226-235.

Disclaimer/Publisher's Note: The statements, opinions and data contained in all publications are solely those of the individual author(s) and contributor(s) and not of MDPI and/or the editor(s). MDPI and/or the editor(s) disclaim responsibility for any injury to people or property resulting from any ideas, methods, instructions or products referred to in the content.